Response of Boost Converters Under Fission-Spectrum Neutron and Gamma Radiation

M. Niichel, T. Miller, B. Jowers III, R. Cooper, and S. Chatzidakis

Abstract—**Radiation testing of microelectronics remains essential for ensuring reliability in environments such as space and nuclear power systems. One critical component found in many systems is the metal oxide semiconductor field-effect transistor (MOSFET). While work has been conducted on early MOSFET designs, there remains a gap in three key areas: testing modern power MOSFETs, collecting live test data, and evaluating components in combined radiation environments. Using modern components ensures that systems currently in use, both public and private, are better protected against radiation damage. Live monitoring allows observation of single-event effects and transient behavior not detectable through post-irradiation analysis. Additionally, conducting experiments in fission-spectrum neutron and gamma environments better replicates real-world conditions. While the literature addresses each of these topics separately, this work combines them by live-testing a boost converter circuit composed of a MAX1932 gate driver and a BSS119N N-type MOSFET under both neutron and gamma radiation. Testing was performed at the Purdue University Reactor Number One (PUR-1) and the Hopewell cobalt-60 irradiator, evaluating the circuit's response to gamma total ionizing dose (TID) and thermal neutron-induced transients. Live monitoring displayed real-time transients, degradation, and recovery behavior. Results indicate gamma radiation plays a dominant role in circuit degradation. However, when considering the dose-dependent degradation, the combined radiation environment of PUR-1 induces failure with 34.8% less dose when compared to the Co-60. Suggesting neutron activation is contributing to secondary gamma dose or boron-10 (n,α) reaction damage. While Co-60 testing remains critical, thermal neutron facilities may offer a useful, cost-effective screening method for identifying gamma-sensitive components.**

Index Terms—**Radiation testing, boost converter, MOSFET degradation, total ionizing dose (TID), neutron activation, thermal neutrons, gamma irradiation, annealing, live monitoring, PUR-1, Co-60 irradiator, microelectronics reliability.**

I. INTRODUCTION

RADIATION testing of microelectronics is increasingly relevant as modern electronics pervade a number of critical systems that operate in harsh environments. This is in tension with some commonly held misconceptions within the microelectronics industry that components have become less susceptible to radiation over time [1], [2]. This is not an unfounded claim, as many efforts have been taken to mitigate radiation induced upsets in a variety of electrical components through manufacturing processes or conformal coatings [3], [4]. However, much of the work has focused on the component level and has lacked diversity in the radiation environment considered. Furthermore, most publicly available work emphasizes simulation derivations over experimental data.

While a radiation-induced failure at the component level cannot be discounted, entire systems have a rich interplay of multiple time-scale effects on the integrated components [5]. As a result, the radiation-induced event may appear significantly different to the end-user than simply an open-circuit or a short-circuit response observed in an individual component. While ultimately the designer cares about the most susceptible element, the end-user cares about how their experience is affected and what performance can be expected out of a device subjected to a radiation environment.

Direct current converter circuits are found in a multitude of electronics, from telecommunications to the power grid. Boost converters act as a means of stepping up direct current voltage for power applications. They act analogously to the alternating current step-up transformer. Due to their widespread use in both space and nuclear power systems, boost converter circuits provide an excellent case study for the propagation of induced effects in a combined neutron and gamma radiation environment [6], [7].

The interest in combined environments stems from realistic operating conditions, such as digital sensors used for instrumentation and control of reactors, space missions, or weapon detonation. The radiation field in real operating environments is rarely a single particle type, nor is it monoenergetic. Therefore, using both neutrons and gammas for system evaluation moves laboratory testing closer to a scenario in which systems would be subjected to during operation. One of the objective problems with this type of evaluation is attributing the effects to each particle. As a result, efforts are made to recreate the experiment in environments of solely neutrons or gammas. However, neutron interactions with matter produce secondary gammas, which are difficult to isolate from the testing system.

II. BACKGROUND

It has recently been demonstrated by El-Azeem and El-Basit that Co-60 gamma radiation significantly degrades the

performance of similar MOSFET-based boost converters [8]. This work implemented a C2M0280120D SiC MOSFET and focused on the switching characteristics of the FET, the change in drain current, and the variation in circuit capacitance as a function of gamma dose up to 600 krad(Si). Unfortunately, they did not consider neutron effects. Similar to other literature, the threshold voltage (V_{TH}) decreases for an enhancement-type FET device [9]. This results in a MOSFET used as a switch to “turn on” for a lower applied gate voltage (V_g). The drain current is also noted to increase as a function of dose. This signifies the decrease in resistance value across the drain to source (R_{DS}). In the “off” state, a large R_{DS} is desired to maintain the integrity of the switching effect. Finally, the circuit capacitance has been identified as increasing with dose [8], [10]. This value results in a reduced ripple voltage across the boost converter output. While the other two effects are typically regarded as negative, the reduced ripple can be beneficial for applications where a steady output voltage is required. It is important to note that El-Azeem and El-Basit did not consider live radiation monitoring. Rather, circuits were subjected to various doses and then measured post-exposure [8].

In 2002, Adell *et al.* classified the effects of total ionizing dose on power MOSFETs [11]. They recognized that significant work had been conducted on classical MOSFETs, but at the time, more work was required to understand power MOSFETs. They considered both boost and buck converter operation post-exposure to a dose of 100 krad(Si) of X-rays. They reported that the mode of operation of the converter circuit affected the rate of degradation of circuit performance. Where boost converters drastically underperformed buck converters when compared to no dose. This was supported by the change in the circuit output voltage (V_{out}) and FET V_{TH}. They also identified that the most limiting component for single-event transients in the circuit was the pulse width modulation (PWM) V_g driver. Simulations and experimental results described the V_{out} of both circuit types decreasing with more noise induced into the PWM driver.

In 2017, Lv *et al.* considered the effect of both fast and thermal neutrons on the optical changes in the material and electrical defects in gallium-nitride-type (GaN) PIN diode commonly found in radiation detectors [12]. While not a MOSFET, PIN diodes are increasing in popularity as power rectifying semiconductors. They noted that while both thermal and fast neutrons induce damaging effects, thermal neutrons disrupted the device more electrically and fast neutrons materially when compared to unirradiated devices.

A foundational finding from previous literature states that many off-the-shelf components can receive 15 krad(Si) of gamma TID before failure. There is little publicly available information on neutron data for similar components. It was proposed that the combined radiation environment would induce synergistic effects on the device under test (DUT) [13].

It is also important to distinguish the damage mechanism between neutrons and TID. A key finding reported by Ashraf in 2018 is that MOSFET carrier mobility (μ) increases with lower concentrations of doping agents in MOSFETs. This finding is useful for describing one mechanism of failure for the MOSFET. Boron, which is commonly found as a p-type dopant, has an isotopic abundance of 20% B-10. This particular isotope has a high affinity for thermal neutrons (~3837 b). In the presence of a thermal neutron field, B-10 undergoes a neutron-alpha reaction. The alpha goes on to induce secondary reactions, but in particular, the dopant density decreases as a function of time within a neutron field [14], [15]. The combination of neutron interaction and dopant reduction stands to reason that there exists a relationship with carrier mobility and neutron flux.

Conversely, TID asymmetrically affects the oxide layer between a MOSFET gate and drain-source junction. In addition to depositing parasitic charges into the junctions, which can affect steady-state and switching characteristics. This mechanism was widely explored by Shashi *et al.* in 2018. They report that the TID tends to increase the capacitance of the oxide (C_{ox}) layer in MOSFETs [16]. This observation is confirmed in a similar work conducted by Yan *et al.* in 2024 [17].

The combination of the neutron and TID effects can be used to describe the change in the MOSFET drain current (I_D) using equations (1) for the linear region and (2) for the saturation region of an n-type MOSFET. The following relationships are,

$$I_D = \frac{\mu C_{OX}}{2}\frac{W}{L}\left[2(V_{GS} - V_{TH})V_{DS} - V_{DS}^2\right] \quad (1)$$

$$I_D = \frac{\mu C_{OX}}{2}\frac{W}{L}\left[2(V_{GS} - V_{TH})^2\right] \quad (2)$$

where, *W* and *L* are the MOSFET channel length. V_{GS} is the gate voltage, V_{DS} is the drain-source voltage, and V_{TH} is the MOSFET threshold voltage. One challenge in a mixed field is separating the effects due to the neutrons and gammas. As both particles cause an increase in I_D. Where neutrons are especially challenging, given that they rarely exist without gamma radiation. However, a neutron energy discrimination can be performed using cadmium to filter out the thermal neutrons, which decreases the probability of neutron interactions with boron.

In summary, extensive work has been conducted to classify the radiation-induced effects on MOSFETs; however, the studies discussed may be missing the full spectrum of effects by not conducting live monitoring or considering combined radiation environments [18]. This article aims to explore the use of live monitoring and combined radiation environments to better understand how circuits fail in real-time and in an environment that more closely resembles operational conditions.

III. Experimental Setup

The following evaluations focus on the Maxim MAX1932 driver and a converter circuit using the commercially available BSS119N N-type silicon MOSFET. These evaluations include monitoring the output voltage of the boost converter circuit as a function of radiation exposure in a pure gamma and fission field. The full component-level diagram for the boost converter circuit is shown below in Fig. 1. Excluded from the diagram is the STM32WLE5JC ARM Cortex that is used to initialize the MAX1932 and provide the clock signal for the diagram shown in Fig. 1.

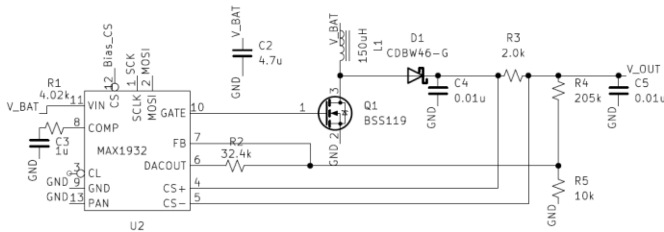

Fig. 1 Component-level schematic of MAX1932 and BSS119N MOSFET boost converter circuit [25].

There are numerous challenges associated with conducting radiation tests in general. However, another set of obstacles is presented while attempting to collect live results while under irradiation. One issue is protecting the recording instruments from the effects of ionizing radiation. The measurement methods for this device are derived from the IEEE standard 802.3af (Power over Ethernet) and are monitored using Arduino hardware and MATLAB-based software [19]. Where, Fig. 2 displays the receiving module and voltage dividers used to collect analog signals from the boost-converter, separated by a 15.2 m Cat5e cable. It is important to note that other diagnostic signals were collected simultaneously using USB USART, but are not discussed in this paper.

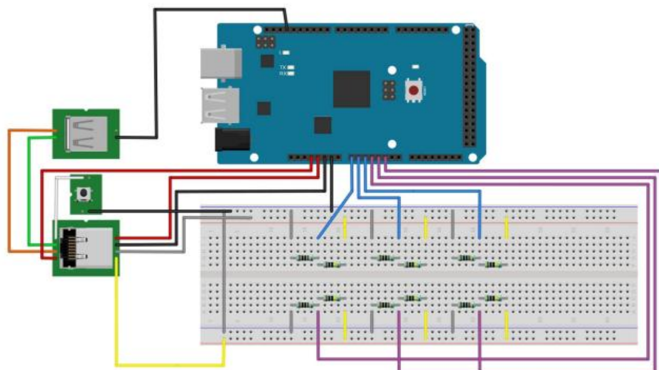
Fig. 2 Component diagram of the remote monitoring setup used to collect analog signals outside of radiation environments.

Radiation Environments

A. Selection Criteria

The selection of the radiation environments to conduct tests had three criteria. Foremost, availability was of chief concern. The second selection criterion was how well each source was characterized for the radiation environment. Finally, the source strength of the environment was used to rule out certain facilities. If it would take an unreasonable amount of time to conduct a test to MIL-STD-750D, the source was excluded [20]. As a result, two facilities were selected. The Purdue research reactor (PUR-1) and the NSWC Crane Co-60 Hopewell irradiator.

B. Purdue Reactor Number One (PUR-1)

The 10-kW research reactor hosted at Purdue University contains a 7.6 cm diameter PVC drop tube that allows for limited irradiation tests. The position of the drop tube allows a test sample to be placed at the midline and a straight-line distance of 30.0 cm from the core.

Gold foil and cadmium cover tests were conducted following ASTM standard E262-17 to determine the thermal and epithermal neutron flux in the drop tube for the reactor at 60% power [21]. The thermal neutron flux was found to be 2.78 × 10^7 cm^{-2} × s^{-1}and the epithermal neutron flux 2.49 × 10^5 cm^{-2} × s^{-1} [21].

It should be noted that it is typical to report neutron fluence as 1-MeV equivalent (Si) for radiation hardness testing. This process is outlined in ASTM E277-09, and the relationship is

$$\Phi_{eq,silicon} = \frac{\int_0^{\infty} \Phi(E)\, F_{D,silicon}(E) dE}{F_{D,Eref,silicon}} \quad (3)$$

where, $\Phi(E)$ is the incident neutron fluence spectrum, $F_{D,Silicon}(E)$ is the energy-dependent displacement damage in silicon, and $F_{D,Eref,Silicon}$ is the neutron displacement reference value (95 MeV × mbarn for silicon) [22]. The neutron fluence spectrum within the core was calculated using MCNP6.3 to produce the neutron lethargy as a function of energy [23]. Fig. 3 displays the neutron lethargy found at the center of PUR-1, and Fig. 4 displays the silicon microscopic displacement Kerma factor as a function of energy. Using equation (3), the 1 MeV equivalent fluence in PUR-1 is 8.32 × 10^{-5} cm^{-2} per source particle. The value can be used to estimate the Flux at the drop tube location using

$$\phi_{tube} = \frac{\Phi_{eq,silicon} P \nu}{E_f 4\pi r^2} \quad (4)$$

where, ϕ_{tube} is simulated neutron flux at the test location, P is the reactor power in watts, ν is the neutron reproduction factor (2.43 for uranium-235), E_f energy per fission in joules, and r is the radius from the reactor. Using equation (4), the 1 MeV equivalent flux at the test location is estimated to be 3.35 × 10^6 cm^{-2} × s^{-1}. The result lies within the range of experimental measurements, but likely overestimates the neutron flux, as the MCNP calculation was performed within the reactor core and does not account for moderation in the coolant. In this context, the MCNP data serves as a first-order approximation for comparison with gold foil activation measurements.

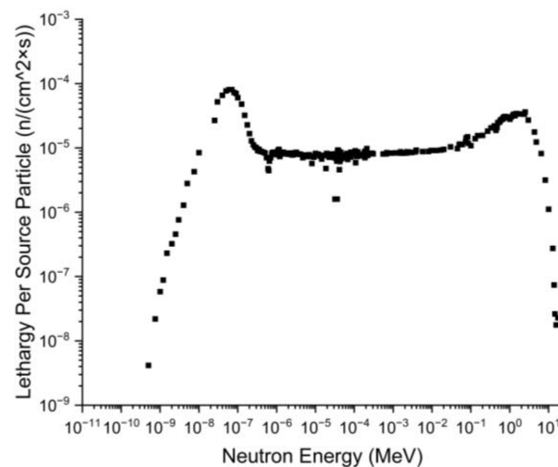

Fig. 3 MCNP PUR-1 neutron lethargy per energy. Note, lethargy allows neutron data to minimize thermal bias.

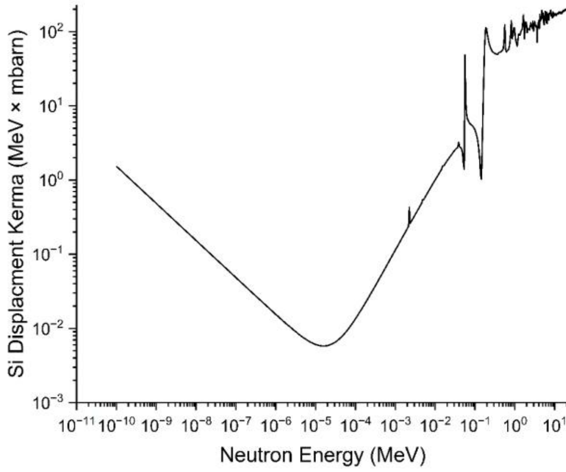

Fig. 4 Silicon microscopic displacement Kerma factor used to determine equivalent fluence.

Multiple $^6LiF_2$ and $^7LiF_2$ thermoluminescent dosimeters were placed in the drop tube at 1% power for 1 minute. Subsequently, the total gamma dose measurement is estimated to be 14.29 rad(Si) (quality factor of 1), and the neutron dose is 1.32 rad(Si) (quality factor of 10). Linear extrapolation for time is then used, given a constant reactor power of 59.94% ± 0.84% measured through the PUR-1 instrumentation. This interpolation can be used to determine the total ionizing dose or the total thermal neutron fluence for any test irradiation time. On average, it was determined that for a 60-minute run at 60% PUR-1 power, the TID is 51.47 krad(Si) and the neutron dose is 4.68 krad(Si).

C. *Hopewell Cobalt-60 Irradiator*

The Hopewell irradiator contains a central well with a concentric ring of Co-60, which is used to expose gamma rays to a device under test. MIL-STD-750D specifically calls for radiation testing to use cobalt-60 due to the large gamma photopeaks of 1.17 MeV and 1.33 MeV.

The military standard also describes the ionizing dose in silicon to exist between 50 and 2000 rad/s(Si). Like the 1MeV equivalent neutron fluence, the TID range is based upon a strategic radiation spectrum. The Hopewell irradiator provides a dose in silicon that adheres to MIL-STD-750D.

IV. Control Measurements

The ultimate goal of the boost converter is to increase the V_{out} from 5 V_{DC} to 34.8 ± 1.2 V_{DC}. While the MAX1932 and BSS119N MOSFETs are capable of providing up to 100 V_{DC}, the particular configuration was selected to power a silicon photomultiplier rated for 35 V_{DC} [24], [25]. Collecting the controlled circuit response and the response to an elevated environmental temperature was of chief concern for evaluating degradation due to radiation effects. Fig. *5* shows several control measurements taken at room 25°C, across V_{out} for the boost converter to establish both the stability and average value. Under nominal conditions, the MOSFET gate is dynamically biased using 3.3 V applied to the MAXIM1932 driver. The hexadecimal code applied is "FF," corresponding to a maximum switching frequency of 360 kHz [24]. The output voltages from the boost converter circuit across capacitor 5 labeled in Fig. 1, were digitally recorded, which provides measurements at discrete values.

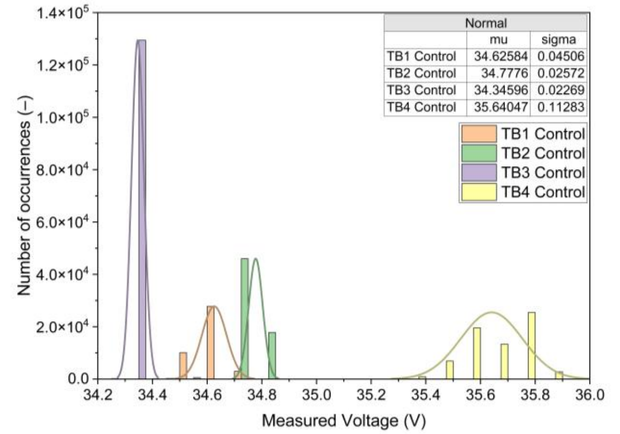

Fig. 5 Distribution of pre-irradiation control measurements of V_{out} for the four test boards at 25°C. The sampling period is 3.4 seconds per measurement. The data for each control were fit to a normal distribution, and the fit parameters are provided in the table. Dynamic bias: MAX1932-based supply, 3.3 V input, 360 kHz switching.

V. Radiation Testing

A. *Combined Neutron and Gamma Environment*

The objective of radiation testing was to conduct live monitoring for three hours within the PUR-1 reactor or until the DUT was no longer able to provide measurable signals. PUR-1 was brought up to 60% power (6 kW) before placing the DUT into the drop tube, then lowered to the testing location. This practice ensures that the gamma dose and neutron fluence can be reasonably predicted using a linear relationship with time.

A series of 7 test boards was placed into PUR-1, surviving for an average of 60 minutes with a maximum time of 72 minutes and a minimum of 43 minutes. Test boards 6 and 7 evaluated the power cycling of the boost converter. As a result, their time until failure is not included in the average. However, the V_{out} at the time of failure was similar to the first 5 boards. The DUT was considered to have failed when either remote serial communication was lost or when the V_{out} of the boost converter returned to 5 V. Here, 5 V is the same value produced when the MOSFET is in the "off-position" for a long time and the energy in L_1 has been fully discharged.

The measured voltage for test board 2 as a function of neutron fluence is shown in Fig. 6. The general trend of V_{out} was a linear departure from the nominal 34.5 V to 42.0 V, beginning near 30 minutes. Three independent channels are used to collect data for coincidence; the mean of the signals is displayed as the average. Note that the discontinuities in the voltage signify a soft reset of the DUT lasting less than 30 seconds each. Departure from one standard deviation of the nominal voltage relative to the individual board's control measurements occurred for a neutron fluence near 1.00×10^{10} cm^{-2}. Table I provides a summary of the test boards and their failure times.

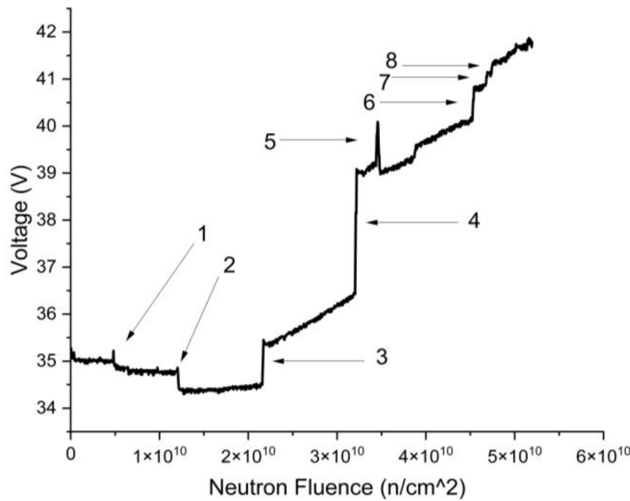

Fig. 6 The mean average of test board 2 V_{out} while subjected to 60% reactor power in PUR-1. Three independent measurements of the voltage were used to generate the mean. Soft resets are numerically labeled. Dynamic bias: MAX1932-based supply, 3.3 V input, 360 kHz switching. Note that the ordinate and abscissa are zero suppressed.

Table I
Summary of Test Board Failures

Test Board Number	Fluence Failure (cm^{-2})	V_{out} Max (V)	Soft Resets
1	7.24×10^{10}	39.4	1
2	1.21×10^{11}	41.7	8
3	8.01×10^{10}	35.2	2
4	1.15×10^{11}	40.6	4
5	1.16×10^{11}	38.8	3
Average	$\mathbf{1.01\times10^{11}}$	**39.2**	**4**
*6	1.35×10^{11}	36.1	1
*7	1.99×10^{11}	40.0	1

Note: Test boards 6 and 7 were used to evaluate boost converter power cycling. Their longevity may not be representative of the remaining boards and has been excluded from the average results.

It was found following test board 3, that a hard reset of the DUT would reestablish serial communication. As a result, post-irradiation measurements were conducted and are displayed in Fig. 7 as a function of time for test board 4. The reduction of the voltage over post-irradiation time occurred in all the boards analyzed following their removal from PUR-1, which suggests some time-dependent annealing. It is important to note that the follow-on measurements were conducted immediately after PUR-1 was scrammed, preventing any unobserved annealing.

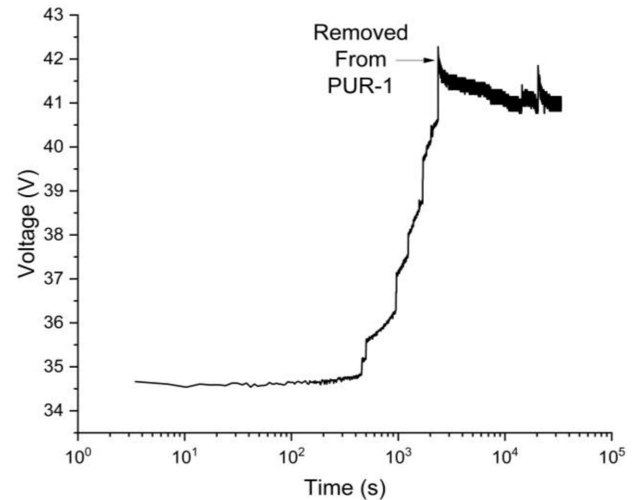

Fig. 7 Test board 4 averaged V_{out} during and following the removal from PUR-1 at 60% power. Dynamic bias: MAX1932-based supply, 3.3 V input, 360 kHz switching. Note that the abscissa is now logarithmic and the ordinate is zero suppressed.

When annealing was observed, it was suggested that there may be a temporal and temperature dependence on self-healing. This has been explored in other literature, but remains different for each component [27]. As a result, it was of interest to test if applied heat would further anneal a test board following an initial annealing period at ambient temperature. An annealing environment cycling from 25°C to 80°C was established. Fig. 8 displays the heating and cooling curve, where the baseline V_{out} is the room temperature annealing value. Though more work is warranted in this area of research, it does not appear that providing a heated environment for an intermediate period appreciably anneals the boost converter system beyond the initial ambient period. This is counter to current literature in that annealing is reasonably expected to heal the MOSFET from TID.

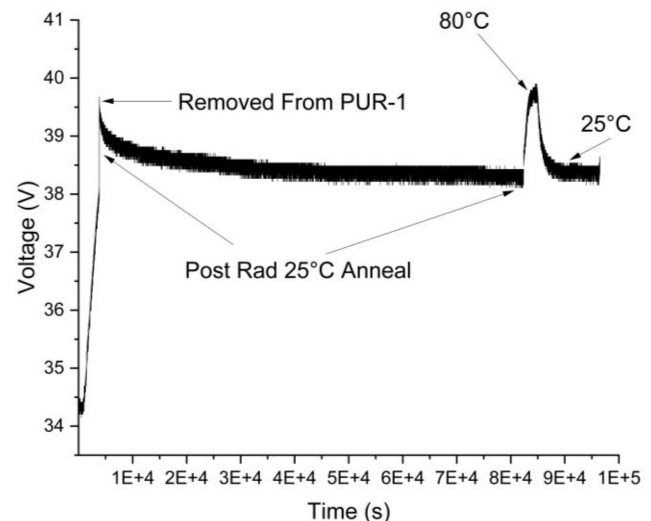

Fig. 8 Test board 8 averaged V_{out} exploring temperature assisted annealing for an 80°C environment cycle. The temperature was held for 30 minutes. Dynamic bias: MAX1932-based supply, 3.3 V input, 360 kHz switching. Note that the ordinate is zero suppressed.

It was also of interest to determine if the effects from PUR-1 could be shifted by filtering out the thermal neutrons using cadmium shielding. The Cd-113 average thermal absorption microscopic cross-section for thermal neutrons is two orders of magnitude larger than the materials that exist in the drop tube. As a result, a 1 mm-thick sheet of cadmium can absorb up to 99.9% of thermal neutrons under 0.55 eV [21]. The remainder of the spectrum that penetrates the shield remains in the epithermal and fast spectrum. However, it should be noted that the capture of the thermal neutrons results in an increased gamma dose from a photopeak at 558 keV [28].

A 0.3 cm-thick cadmium sheet was applied to the drop tube in PUR-1 to effectively remove all of the thermal spectrum in the testing region. Gold foil measurements were once again used to determine the neutron flux. Where foils were placed external and internal to the cadmium shield to measure total and epithermal/fast flux. The respective values for neutron flux at 60% power are 2.63×10^{7} cm^{-2} × s^{-1} (0.27% uncertainty) and 7.48×10^{5} cm^{-2} × s^{-1} (0.54% uncertainty). Furthermore, a secondary TLD was placed under the same condition, which reported the gamma dose and neutron dose of 15.03 rad(Si) and 1.32 rad(Si), respectively. For a 60-minute run at 60% power, the approximate TID is 54.11 krad(Si), and the neutron dose is 4.75 krad(Si).

A boost converter circuit was placed in PUR-1 for 68 minutes, and the V_{out} was recorded (Cd PUR-1). These results are presented and compared to test board 4 (PUR-1) and the Co-60 test board in Fig. 9 as a function of dose. The dose rate for both instances within PUR-1 are derived from the TLD measurement by combining the neutron and gamma dose values.

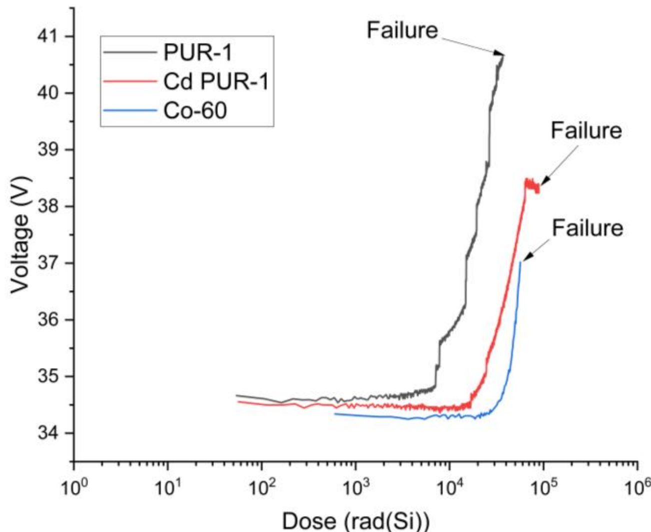

Fig. 9 V_{out} for each radiation environment as a function of gamma dose and estimated gamma and neutron dose for the reactor. Dynamic bias: MAX1932-based supply, 3.3 V input, 360 kHz switching. Note that the abscissa is now logarithmic and the ordinate is zero suppressed.

The BSS119N MOSFET from the boost converter was evaluated following each environment to investigate the shift in the steady-state characteristics. This was to validate that the FET component contributes to the failure of the boost converter. For the given radiation environments, it was found that the devices in the Co-60 and cadmium were shorted from source to drain and could not be evaluated; however, the unshielded PUR-1 MOSFET displayed an increased shift in the saturation mode drain currents by approximately three decades when compared to an unirradiated control. These results are shown in Fig. 10 and Fig. 11 respectively.

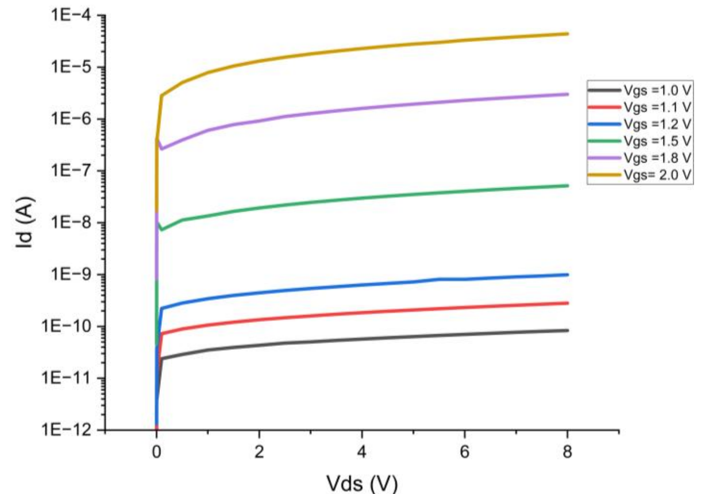

Fig. 10 MOSFET drain current of the control BSS119n. Note that the ordinate is logarithmic.

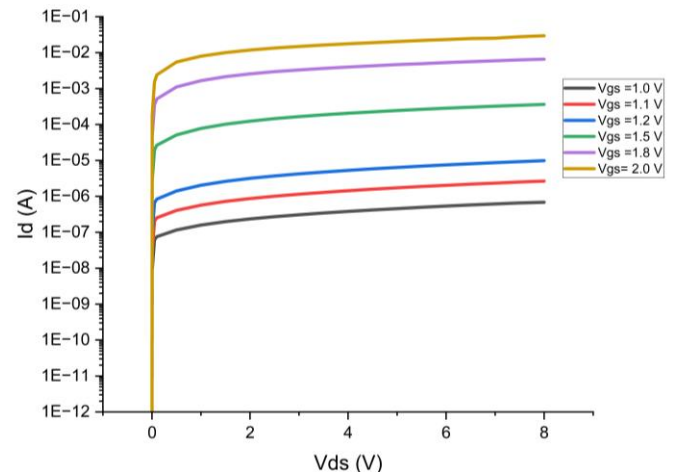

Fig. 11 MOSFET drain current following 60 minutes in PUR-1 at 60% power unshielded. Note that the ordinate is logarithmic.

B. Gamma Environment

The objective of Co-60 TID testing was to assist in isolating the particle responsible for the observed transient in the boost converter circuit. The Hopewell source could observe similar effects as PUR-1, but at a significantly accelerated timeframe when compared to the much longer one-hour runs at PUR-1.

Three test boards were subjected to the Co-60 source, and the average test time to failure was 10 minutes. In accord with PUR-1 reactor tests, the reported V_{out} displayed an exponential increase to 37.0 +0.1/-1.2 V and then failed to the default 5 V

output, indicating a circuit failure. Due to the total failure of the circuit, a post-irradiation assessment considering annealing could not be performed on these test boards. However, it was found that the value R_{DS} read as 0 Ω, indicating a MOSFET burnout. The average V_{out} measurements of the 3 for each of the Co-60 tests are shown in Fig. 12.

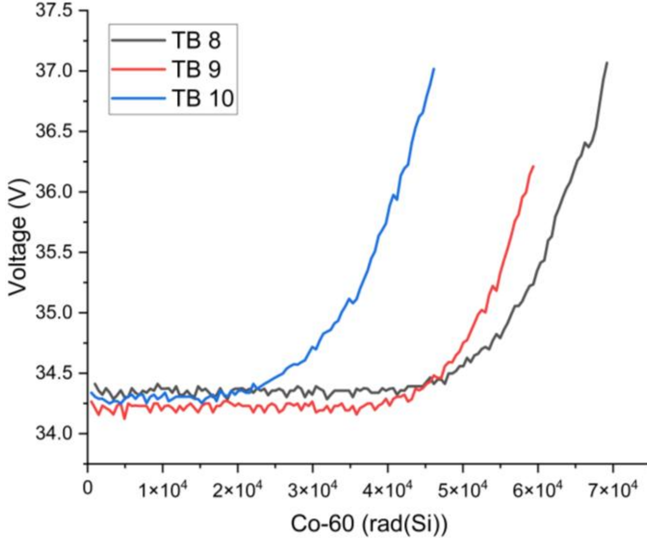

Fig. 12 Recorded V_{out} of boost converters for MIL-STD-750D compliant Co-60 dose rate TID. Dynamic bias: MAX1932-based supply, 3.3 V input, 360 kHz switching. Note that the ordinate is zero suppressed.

VI. DISCUSSION

Upon conducting the TID experiment, evidence supports that the TID has a significantly larger effect on the boost converter output voltage when considering both time in the environment and the destruction of the DUT during irradiation. This was supported by the accelerated time until failure and the inability to conduct post-irradiation measurements. The similar behavior of the output voltage over time and subsequent dose suggests that the induced transient in V_{out} is more affected by gamma radiation than neutrons. However, when the comparison is made as a function of dose, evidence suggests that the combined radiation environment without thermal neutron shielding causes premature failure by 34.8% and early onset damage when compared to the failure dose of the most conservative failure among the Co-60 tests.

For the experimental setup in the drop tube, there is little room to add additional shielding. However, given the thermal shielding effects of cadmium, it can be assumed that at 0.3 mm thickness, the majority of the neutron flux that the shielded test received was greater than 0.55 eV [21]. As a result, the probability of material activation decreases by multiple orders of magnitude for most stable isotopes present, except for the resonance region [29]. We propose that the increased survivability of the shielded experiment is due to reduced neutron activation and subsequent secondary neutron reactions such as (n,γ), (n,p), or (n,α). These results suggest that thermal neutron effects cannot be dismissed. If TID is the source of the effects observed, then it can reasonably be expected that in a thermal flux, the material activation of the DUT may contribute to the ionizing dose. As a result, it is believed that there are synergistic effects from the combined radiation environment that contribute to deposited energy.

Additionally, there is a time dependence of the activation and the production of decay gammas. The placement of the TLDs in the testing location at the start of PUR-1 operation time most likely did not experience any of the additional dose from these activation products. It is proposed that 60 seconds was not long enough for the medium and long-lived isotopes to be generated. The problem associated with the use of TLDs for this measurement is the device's dose saturation point. A few minutes in PUR-1 at 1% power would cause a saturation of the device, without taking into account activation.

One solution is to find a dose measurement device that has a saturation point at multiple krad(Si). However, an alternative solution may be conducting a similar experiment at the end of the one-hour PUR-1 experiment for 60 seconds, as opposed to the beginning. The difference in the recorded dose may provide insight into the contribution from activated materials.

Moreover, due to the proximity of activated components, small activities may have a non-negligible effect on the total dose experienced by the DUT. As a result, it was of interest to future efforts to gather an HPGe gamma spectrum of the DUT immediately following the removal from the neutron flux. Fig. 13 provides the gamma spectrum of the activated board containing the boost converter and accompanying circuits, with the strongest peaks labeled.

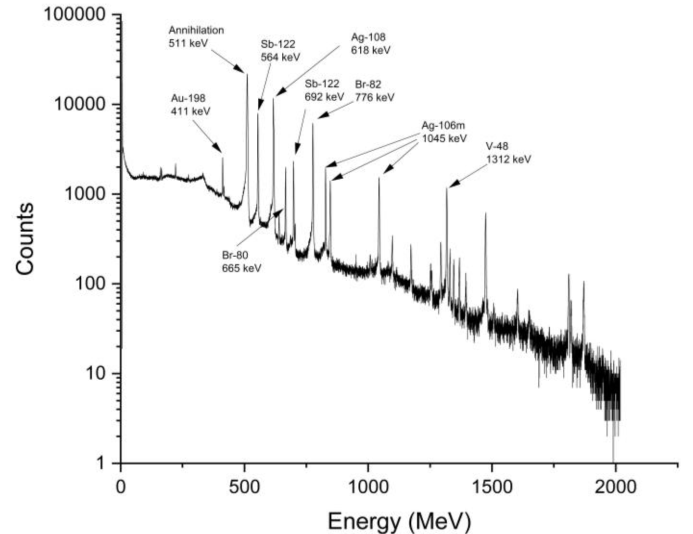

Fig 13. HPGe gamma energy spectrum collected for 600 seconds following a 60-minute exposure in PUR-1. Note that the abscissa is logarithmic.

The gamma spectrum displayed above shows several isotopes that are decaying following neutron activation. This measurement supports that self-irradiation following neutron exposure may not be negligible. While a fast spectrum will induce activation, the probability is lower than in a thermal spectrum. As a result, this must be a consideration for this and other experiments. What is not taken into consideration with an HPGe measurement following removal from PUR-1 is the prompt reactions, which are typically much higher in energies

5-10 MeV and can be used to determine the extent of the B-10 capture in any CMOS devices. Similar to the live-monitoring of the DUT signals, conducting a gamma count during the experiment offers more information regarding the mechanism of damage. Current work is being conducted with university and government collaboration to investigate at power B-10 capture.

The PUR-1 portion of this test does not exclusively rule out effects from displacement damage, nor the effects from thermal neutrons. However, the results in the TID section strongly correlate with the results from PUR-1. This suggests that the effects that are observed under the reactor conditions are primarily from the gammas, rather than the neutrons. It is therefore suggested that a test in a fast neutron spectrum would provide data that could be used in isolating any effects induced by displacement damage.

It is important to consider that the converter circuit did not undergo thermal annealing behavior. As it is well reported in the literature that elevated temperatures release trapped oxide charges. The charges can recombine, thus providing self-healing. The following sequence of events may be used to explain why there is a lack of healing for the DUT following temperature annealing. Radiation exposure of either neutrons or gammas causes a decrease in the MOSFET's V_{TH}, allowing it to remain in conduction for a longer portion of each switching cycle. This effectively increases the MOSFET's on-time and duty cycle, resulting in a higher V_{out} from the boost converter. The MAXIM1932 controller senses this voltage rise through its negative feedback loop and attempts to restore stability by lowering the PWM switching frequency, thereby lengthening the switching period and reducing the duty cycle. However, as radiation continues to lower V_{TH}, the MOSFET's drain current increases, and the controller must further decrease the frequency to maintain regulation. When ΔV_{TH} becomes excessive, the MAXIM1932 reaches its minimum operating frequency, and no longer compensates. At this point, the converter operates near 100% duty cycle, leading to excessive conduction, thermal runaway, and eventual MOSFET failure. Annealing cannot restore normal operation because the radiation-induced V_{TH} degradation exceeds the controller's compensation capability, leaving the feedback loop unable to stabilize the output.

Furthermore, it was of interest to compile a preliminary list of metals for MCNP modeling. A Hitachi EA1400 X-ray fluoroscopy (XRF) machine was used to generate the relative weights on an elemental basis. Fig. 14 displays the MOSFET as observed through the XRF machine, and Table II provides the suggested elements by relative weight and their associated 2200 m/s thermal neutron cross-sections, as determined by Brookhaven National Laboratory in 1992 [30]. It should be noted that the X-ray tube internal to the XRF equipment is made of rhodium. It does not have a self-discriminator, so any rhodium found in the spectrum may be discarded. Additionally, the XRF has a low Z-limitation, where materials with Z values less than 11 are not detectable [31]. Thus, boron is not detectable by XRF. This analysis could not distinguish the effects of the (n,α) reaction of boron-10 and neutron-induced TID.

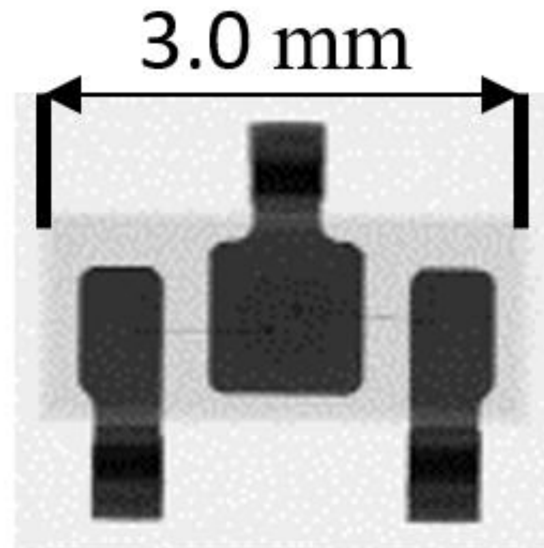

Fig 14. BSS119n MOSFET image generated while under X-ray fluoroscopy.

Table II
XRF Elemental Composition of MOSFET

Element Symbol	Relative Weight (%)	3σ (%)	XS (b)
Si	37.6834	47.138	0.171
Cu	23.4044	17.7039	3.78
Rh	15.9979	12.1015	144.8
Ag	12.9569	9.8011	63.3
Sn	5.0039	3.7859	0.626
Ba	1.8555	1.4247	1.1
Fe	1.0164	0.7693	2.56
V	0.5425	0.4174	5.08
Cr	0.4799	0.366	3.05
Au	0.3307	0.2511	98.65
Sb	0.3023	0.2444	4.91
Zn	0.1972	0.1494	1.11
Ta	0.1688	0.1299	20.6
Ni	0.0489	0.0387	4.49
Br	0.0113	0.0166	6.9

While the results for the cadmium shielded board are not robust at this point, they offer a unique insight into the effects of thermal neutrons on the system. Unlike any of the other boards, there was a period of irradiation during which the results were stable. Due to the gammas from the thermal neutron capture on the cadmium shield, the gamma dose within the shield is 4.87% larger than the bare drop tube. If the transient in V_{out} is solely due to the TID effects, it is hypothesized that the slight uptick in gamma dose from the cadmium shielding should yield similar results or an increased rate of boost converter degradation. However, it is observed that the rate of V_{out} increase is lower, settling at a maximum value of 38.5 V, then settling in a region of stability.

While these results are not definitive enough to disregard MIL-STD-750D tests for fast neutrons or total ionizing dose, there is evidence that thermal sources can cause damage through TID via activation or the prompt (n,γ) reaction. Due to the limited availability of fast-burst reactors and domestically produced Co-60, along with the high cost of testing, it may not always be practical for microelectronics designers and manufacturers to perform these evaluations. This work contends that more available thermal reactors may be used as a primary means of identifying radiation-soft components. A fabricator may then apply current radiation hardening techniques prior to irradiation time in the military standard sources. This effort would save both development time and money for medium- and low-priority systems, which require a radiation-hardened classification. It may also be worthwhile to develop a secondary classification of components that pass thermal and TID testing, but have not been tested for fast neutrons. A lower grade classification would allow for accelerated fielding of components that need to be deployed immediately or for intermediate-length missions.

The work conducted with the cadmium shielding identified the need for future efforts considering various metal shields. At this point, it is hypothesized that a combination or alloy of metals with a high affinity for thermal neutron capture and subsequent high-energy gamma radiation may allow for full capitalization of a thermal source, shifting the effects closer to those of Co-60. Perhaps the neutron flux may not be large enough to provide any evidence of transient behavior. However, the neutrons may be used to maximize the high-energy TID to a test article. While the activity alone may not be large enough to act as an independent source of gammas, a casing around a DUT may provide the proximity necessary to induce TID effects. Efforts are currently underway exploring the use of Nickel, Cadmium, and Gadolinium test casings for their large neutron absorption cross-sections and high-energy gamma production.

VII. Conclusion

This study has demonstrated that the combined radiation environment of thermal neutrons and gamma rays significantly impacts the performance of commercial boost converter circuits, with gamma radiation identified as the primary driver of transient behavior and circuit failure. Results from live monitoring at PUR-1 and the Co-60 irradiator highlight that degradation manifests as an increase in output voltage followed by abrupt circuit failure, typically associated with MOSFET burnout for high TID. Thermal neutron effects, particularly through induced activation, contribute to secondary gamma exposure, potentially compounding TID effects. Cadmium shielding experiments further revealed that attenuation of thermal neutrons leads to deviations in degradation trends, suggesting synergistic interactions in mixed radiation fields. The findings advocate for the use of accessible thermal neutron reactors for early-stage identification of radiation-sensitive electronics, potentially accelerating the development cycle for radiation-hardened systems. Future research should expand on shielding strategies and material activation impacts to better isolate and understand particle-specific damage mechanisms.

Acknowledgment

This work would not be possible without the help of Major David Fobar, United States Army, for his contribution to the SCRAM chip designed under DTRA/NSERC. Additionally, the Purdue Military Research Institute for providing their support towards this research. Furthermore, the United States Navy for Naval NISE/219 funding. Finally, True Miller and Brian Jowers III, Reactor staff, for their MCNP model and operation of PUR-1.

References

[1] A. H. Johnston, “Radiation Effects in Advanced Microelectronics Technologies ”, *IEEE Trans. Nucl. Sci.*, NS-45, 1339 (1998).

[2] A. Cester and A. Paccagnella, “Ionizing radiation effects on ultra-thin oxide MOS structures,” *Int. J. High Speed Electron. Syst.*, vol. 14, no. 02, pp. 563–574, June 2004, doi: 10.1142/S012915640400251X.

[3] S. C. Hanson, Y. Xiao, R. Charrette, and R. B. Hayes, “A preliminary NASA compliant conformal coating for optimized space radiation shielding configurations and its mass attenuation coefficients,” *Prog. Nucl. Energy*, vol. 169, p. 105089, Apr. 2024, doi: 10.1016/j.pnucene.2024.105089.

[4] Y. Q. D. Aguiar, F. Wrobel, J.-L. Autran, and R. García Alía, *Single-Event Effects, from Space to Accelerator Environments: Analysis, Prediction and Hardening by Design*. Cham, Switzerland: Springer Int. Publishing, 2025, doi: 10.1007/978-3-031-71723-9.

[5] C. De Sio, S. Azimi, L. Sterpone, and B. Du, “Analyzing Radiation-Induced Transient Errors on SRAM-Based FPGAs by Propagation of Broadening Effect,” *IEEE Access*, vol. 7, pp. 140182–140189, 2019, doi: 10.1109/ACCESS.2019.2915136.

[6] M. E. Sahin and F. Blaabjerg, “An overview on MOSFET drivers and converter applications,” *Electr. Power Compon. Syst.*, vol. 49, no. 8, pp. 828–847, May 2021, doi: 10.1080/15325008.2021.2002477.

[7] J. J. Liou and F. Schwierz, “RF MOSFET: Recent advances, current status and future trends,” *Solid-State Electronics*, vol. 47, no. 11, pp. 1881–1895, Nov. 2003, doi: 10.1016/s0038-1101(03)00225-9.

[8] S. M. A. El-Azeem and W. A. El-Basit, “Impact of gamma-ray irradiation on commercial silicon carbide MOSFET with boost converter application,” *Power Electron. Devices Compon.*, vol. 10, p. 100077, Mar. 2025, doi: 10.1016/j.pedc.2025.100077.

[9] B. Djezzar, A. Smatti, A. Amrouche, and M. Kechouane, “Channel-length impact on radiation-induced threshold-voltage shift in N-MOSFET devices at low gamma ray radiation doses,” *IEEE Trans. Nucl. Sci.*, vol. 47, no. 6, pp. 1872–1878, Dec. 2000, doi: 10.1109/23.914462.

[10] Z. An *et al.*, “The impact of TID effect on EMS of PDSOI voltage reference circuits,” in *2018 IEEE International Symposium on Electromagnetic*

Compatibility and 2018 IEEE Asia-Pacific Symposium on Electromagnetic Compatibility (EMC/APEMC), Singapore: IEEE, May 2018, pp. 852–856. doi: 10.1109/ISEMC.2018.8393902.

[11] P. C. Adell *et al.*, “Total-dose and single-event effects in switching DC/DC power converters,” *IEEE Trans. Nucl. Sci.*, vol. 49, no. 6, pp. 3217–3221, Dec. 2002, doi: 10.1109/TNS.2002.805425.

[12] L. Lv *et al.*, “Fast and Thermal Neutron Radiation Effects on GaN PIN Diodes,” *IEEE Trans. Nucl. Sci.*, vol. 64, no. 1, pp. 643–647, Jan. 2017, doi: 10.1109/TNS.2016.2630061.

[13] D. J. Cochran, “Recent total ionizing dose and displacement damage compendium of candidate electronics for NASA space systems,” in *Proc. IEEE Radiat. Effects Data Workshop*, Jul. 2011, pp. 1–10.

[14] N. S. Ashraf and K. Iniewski, *Low Substrate Temperature Modeling Outlook of Scaled N-MOSFET*, no. #10. San Rafael: Morgan & Claypool Publishers, 2018. doi: 10.1007/978-3-031-02034-6.

[15] E. C. Auden *et al.*, “Thermal Neutron-Induced Single-Event Upsets in Microcontrollers Containing Boron-10,” *IEEE Trans. Nucl. Sci.*, vol. 67, no. 1, pp. 29–37, Jan. 2020, doi: 10.1109/TNS.2019.2951996.

[16] S. Bala, R. Kumar, and A. Kumar, “Total Ionization Dose (TID) Effects on 2D MOS Devices,” *Trans. Electr. Electron. Mater.*, vol. 22, no. 1, pp. 1–9, Feb. 2021, doi: 10.1007/s42341-020-00255-3.

[17] Z. Yan *et al.*, “Impact of Total Ionizing Dose on Radio Frequency Performance of 22 nm Fully Depleted Silicon-On-Insulator nMOSFETs,” *Micromachines*, vol. 15, no. 11, p. 1292, Oct. 2024, doi: 10.3390/mi15111292.

[18] D. M. Fleetwood and H. A. Eisen, “Total-dose radiation hardness assurance,” *IEEE Trans. Nucl. Sci.*, vol. 50, no. 3, pp. 552–564, June 2003, doi: 10.1109/TNS.2003.813130.

[19] M. Niichel, “Development Of An Electronics Testbed For Radiation Testing In Gamma And Neutron Environments,” M.S. thesis. Purdue University, West Lafayette, IN, 2024.

[20] U.S. Dept. of Defense, “Test methods for semiconductor devices,” *MIL-STD-750*, Feb. 23, 1983. [Online]. Available: https://www.navsea.navy.mil/Portals/103/Documents/NSWC_Crane/SD-18/Test%20Methods/MILSTD750.pdf

[21] ASTM International, “Standard test method for determining thermal neutron reaction rates and thermal neutron fluence rates by radioactivation techniques,” *ASTM E262-17*, 2017. [Online]. Available: https://www.astm.org/e0262-17.html

[22] ASTM International, “Standard practice for characterizing neutron fluence spectra in terms of an equivalent monoenergetic neutron fluence for radiation-hardness testing of electronics,” *ASTM E722-09*, Dec. 2010.

[23] J. A. Kulesza *et al.*, *MCNP® Code Version 6.3.0 Theory & User Manual*. (Sept. 2022). Los Alamos National Laboratory Tech. Rep., Los Alamos, NM, USA.

[24] Maxim Integrated Products, “MAX1932 digitally controlled, 0.5% accurate, safest APD bias supply,” 2019. [Online]. Available: https://www.analog.com/media/en/technical-documentation/data-sheets/max1932.pdf

[25] Infineon Technologies AG, “OptiMOS™ Small-Signal-Transistor.” 2012. [Online]. Available: https://www.mouser.com/datasheet/2/196/Infineon-BSS119N-DS-v02_01-en-773952.pdf

[27] V. Danchenko, U. D. Desai, and S. S. Brashears, “Characteristics of Thermal Annealing of Radiation Damage in MOSFETs,” *Journal of Applied Physics*, vol. 39, no. 5, pp. 2417–2424, Apr. 1968, doi: 10.1063/1.1656570.

[28] J. W. Mietelski, “Detection of background thermal neutrons in a modified low-background germanium gamma-ray spectrometer,” *J Radioanal Nucl Chem*, vol. 322, no. 3, pp. 1331–1339, Dec. 2019, doi: 10.1007/s10967-019-06843-9.

[29] J. Sublet, J. A. Simpson, R. A. Forrest, and D. Nierop, “NGAtlas,” Int. Atomic Energy Agency, Sept. 2001. [Online]. Available: https://www-nds.iaea.org/ngatlas2/atlas.htm[30] V. F. Sears, “Neutron scattering lengths and cross sections,” *Neutron News*, vol. 3, no. 3, pp. 26–37, Jan. 1992, doi: 10.1080/10448639208218770.

[31] “An introduction to X-ray fluorescence (XRF) analysis in archaeology,” in *X-Ray Fluorescence Spectrometry (XRF) in Geoarchaeology*, New York, NY, USA: Springer, 2011, pp. 7–44, doi: 10.1007/978-1-4419-6886-9_2.